Proceedings of the 17th World Congress
The International Federation of Automatic Control
Seoul, Korea, July 6-11, 2008

A whole body model of FDG metabolism based on VHP datasets

Jing, Bai, Huiting, Qiao

**Dept. of Biomedical Engineering, School of Medicine, Tsinghua University, Beijing, 100084, China (e-mail: deabj@tsinghua.edu.cn).*

Abstract: Using 2-[^{18}F]fluoro-2-deoxy-D-glucose (FDG) and positron emission tomography (PET), the kinetic models for FDG metabolism were established in tissue of myocardium, lung, stomach, spleen, pancreas, marrow, liver and kidneys. All submodels were connected by the circulation system, forming the whole body model. The model can be visualized on the base of Visible Human Project (VHP), to simulate the dynamic metabolic process of FDG in human body. The simulated FDG distribution images were in 2D and 3D formats, and presented higher resolution than original PET image. The result of this study can be used not only for education and related research, but also by PET operators to design their PET experiment program.

1. INTRODUCTION

The development of Positron Emission Tomography (PET) makes it possible to detect the metabolic process in human body. 2-[^{18}F]fluoro-2-deoxy-D-glucose (FDG) is the analog of glucose, which is widely used in clinical PET experiments (Gallagher et al., 1977; Kostakoglu et al., 2003). Some FDG kinetic models for organs were established to understand the metabolism of glucose and to help better detect disease (Huang et al., 1980; Bertoldo et al., 1998; Reinhardt et al., 1999). The kinetic models for gray matter, white matter, skeletal muscle, and myocardium have been established. However to understand the whole body metabolism, these models are far from adequate. Therefore more kinetic models, such as the models for lung, stomach, spleen, pancreas, and marrow, have been developed (Cui et al., 2006).

Due to the physiological characteristics of some tissues such as liver and kidneys, particular models have been developed for them. The liver has a dual blood supply from the hepatic artery (HA) and the portal vein (PV). Thus, the dual-input model was employed for liver (Cui et al., 2007a). It was experimentally confirmed that the dual-input function may lead to more accurate parameter estimation. As for kidney, the high quantity excretion of FDG makes its metabolic process inconspicuous (Szabo et al., 2006). Classic three-compartment model can not well explain FDG excretion from kidney well. Thus, the model for kidneys was developed.

Hays and Segall (1999) have proposed a whole-body model which includes brain, myocardium, liver, and lung. In this model, all individual tissue's models were connected to each other through their common compartment --the blood compartment. However, as mentioned in their study, the whole-body model included only 24% of FDG metabolism in human body because many other tissues which were active in metabolism of FDG were not involved in this model. To improve such a whole body model, submodels for stomach, spleen, pancreas, marrow, liver and kidneys were developed and connected to each other.

The function information from the whole body model incorporated with anatomical information can be visualized. The Visible Human Project (VHP) provides a set of detailed anatomical information of human body and has been widely used in the medical imaging segmentation, reconstruction, and 3D visualization (Hohne et al., 2001; Pommert et al., 2001; Jastrow et al., 2003). In this study we assigned the TAC obtained from whole body to the segmented VHP image frames. Thus a set of dynamic volume data for FDG distribution was simulated, and the simulated FDG distribution was visualized by volume rendering method (Cui et al., 2007b).

In this paper, the development of the model and the simulation were introduced respectively in following sections. The whole body model was developed as well as the models for liver and kidneys were proposed. And the method of visualization was described in detail.

2. MODEL OF FDG METABOLISM

In order to model the normal metabolic process in human body, sixteen normal volunteers participated in the study. They were divided into two groups to take dynamic PET experiment. For group one (six volunteers), the study was performed in a single bed position covering from upper heart to lower liver. For group two (ten volunteers), the study was performed in a single bed position covering kidney. The data derived from dynamic FDG-PET experiments were used to model metabolic process in each tissue.

2.1 Compartment model

Three-compartment model (Fig. 1) has been used to describe FDG metabolism in many tissues such as gray matter, white matter, myocardium, and skeletal muscle. This classic model was also used here to describe the FDG metabolic process in

the tissues of lung, liver, stomach, spleen, pancreas, and marrow.

In this model, the left compartment represents vascular space for FDG, the center compartment represents tissue space for free FDG and the right compartment represents tissue space for FDG-6-phosphate (FDG-6-P). The concentrations of FDG or FDG-6-P in the three compartments are C_B, C_E, and C_M, respectively. The model parameters k_1~k_4 are the rate constants of material exchange between compartments. Since the radioactivity of ^{18}F is easy to detect and convert to FDG concentration, the time activity curve (TAC) were used to express FDG concentration function, for example blood time activity curve (BTAC) is the input of the model as $C_B(t)$. In this compartment model, $C_T(t)$, the observed total tissue time activity curve (TTAC) in PET image can be described as following equations:

$$C_T(t) = C_E(t) + C_M(t) + f \cdot C_B(t) \tag{1}$$

$$C_T(t) = \frac{k_1}{\alpha_2 - \alpha_1}\left((k_3 + k_4 - \alpha_1)e^{-\alpha_1 t} + (\alpha_2 - k_3 - k_4)e^{-\alpha_2 t}\right) \otimes C_B(t) + f \cdot C_B(t) \tag{2}$$

where $\otimes$ denotes the operation of convolution, f is the spillover fraction from blood to the tissue and

$$\alpha_1 = \left(k_2 + k_3 + k_4 - \sqrt{(k_2 + k_3 + k_4)^2 - 4k_2k_4}\right)/2 \tag{3}$$

$$\alpha_2 = \left(k_2 + k_3 + k_4 + \sqrt{(k_2 + k_3 + k_4)^2 - 4k_2k_4}\right)/2 \tag{4}$$

In general, this compartment model for FDG-PET requires the measurements of both BTAC and TTAC, which are input and output functions of the model. The parameters k1~k4, together with spillover fraction f, are estimated by fitting the output function of the model.

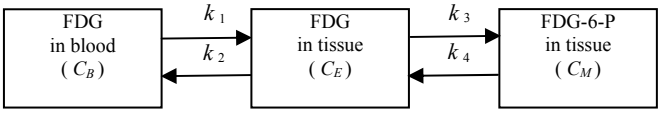

Fig. 1. The three-compartment model for FDG metabolism

Despite most tissues can be described by this three-compartment model, the organs such as liver and kidneys will not be well described by this model.

2.2 Dual-input model for liver

Unlike other tissues, the liver has a dual blood supply from the hepatic artery and from the portal vein. The single arterial-input may be not consistent with the actual model input in the liver model, and the use of arterial-input may introduce errors in the estimated model parameters (Munk et al., 2001). Therefore, a dual-input function, which was generated by calculating weighted sum of both the arterial and the portal vein input curve, was used in liver model (Chen and Feng, 2004). The proportion of the two blood supplies was

$$C_B(t) = C_a(t) \times 20\% + C_v(t) \times 80\% \tag{5}$$

where $C_a(t)$ was BTAC derived from region of aortas and $C_v(t)$ was BTAC derived from region of portal veins. Though portal veins are small in size, they are still distinguishable in early scan, so dual-input liver model is also noninvasive. For liver model, the kinetic parameters were estimated using dual-input and arterial-input respectively. In comparison with the arterial-input function, the dual-input function generates a better fit for the liver model. Moreover, it is also compatible with the clinical physiology.

2.3 Piecewise model for kidney

Kidney is a special tissue in the body. Since FDG can not be reabsorbed at renal tubule, great quantity of FDG flows out of the body through kidney. The high quantity excretion of FDG makes its metabolic process inconspicuous, viz. the processes of phosphorization and dephosphorization are neglected. A unidirectional compartment was described piecewise for kidney, illustrated in Fig. 2.

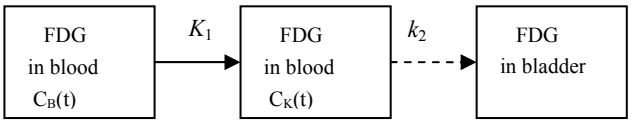

Fig. 2. The unidirectional compartment model for kidney

This kidney model was divided into two parts by a new parameter t_0: one part described the accumulation process before t_0, and the other described the excretion process of FDG in kidney. t_0, the timing delay constant, was the time point when FDG began to excrete from kidney. K_1 and k_2 were the rate constants of FDG between each compartment. When $t<t_0$, FDG diffused in blood, went into the kidney from circulation system, and was filtrated to urine and accumulated in kidney temporarily. When $t> t_0$, it began to excrete FDG with urine out of the kidney.

Ten sets of dynamic clinical data were used to estimate the parameters K_1, k_2, f and t_0. Results have shown some differences in each subject. However, the output of the model fitted with the original curve from clinical data well, and the excretion of FDG calculated from our model did not differ significantly from the published results using other methods.

2.4 Whole body model

The circulatory system connected each individual tissue's model, and formed a distributed whole-body model (Fig. 3). In addition to the tissues investigated in this study, the existent gray matter, white matter and skeletal muscle models were incorporated into this model. The whole body model can describe the metabolism character of major tissues.

With the BTAC and TTAC derived from sixteen sets of dynamic imaging, the model parameters were estimated by the weighted nonlinear least square (WNLS) method, and list in Table. 1.

Table 1. Parameters of the model

	K1 (ml/min/ml)	k2 (min-1)	k3 (min-1)	k4 (min-1)	f
Myocardium	0.196±0.115	1.022±0.504	0.149±0.115	0.010±0.011	0.545±0.099
Lung	0.014±0.009	0.291±0.158	0.006±0.006	0.000±0.000	0.151±0.025
Liver’	1.256±0.160	1.329±0.266	0.002±0.001	0.002±0.004	0.165±0.066
Stomach	0.614±0.218	1.885±0.538	0.071±0.023	0.031±0.009	0.063±0.023
Spleen	1.207±0.498	1.909±0.471	0.008±0.006	0.014±0.011	0.000±0.000
Pancreas	0.648±0.365	1.640±0.873	0.027±0.024	0.016±0.015	0.107±0.121
Marrow	0.425±0.179	1.055±0.427	0.023±0.006	0.013±0.005	0.040±0.025
Kidney’’	0.263±0.065	0.299±0.064			0.438±0.156
Gray matter’’’	0.102±0.028	0.130±0.066	0.062±0.019	0.007±0.002	
White matter’’’	0.054±0.014	0.109±0.044	0.045±0.019	0.006±0.002	
Skeletal muscle’’’	0.047±0.024	0.325±0.273	0.084±0.045	0.000±0.000	0.019±0.019

’ using dual-input model
’’ using new kidney model, t_0 is 3.63±0.77 (min)
’’’ the parameters of gray matter, white matter and skeletal muscle are referenced from literature

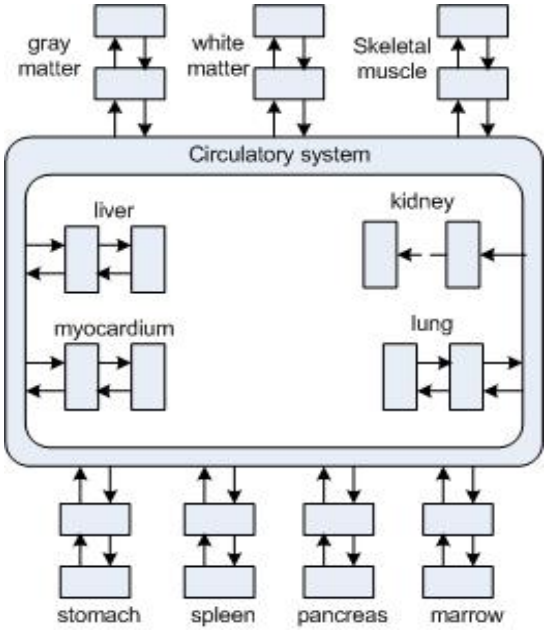

Fig.3. Whole body model

3. SIMULATION AND VISUALIZATION

With the whole body model, the distribution of FDG in human body could be simulated, and the dynamical process could be visualized with high resolution and high quality on the base of VHP dataset. With a BTAC from FDG-PET experiment, the TTACs of each main metabolism tissue were simulated, which represented the ^{18}F distribution processes. VHP dataset, which provided anatomical information, was used for the high resolution 3D visualization of ^{18}F distribution process in human body (Cui and Bai, 2005). First, a sequence of activity values of each tissue was obtained by discrete time sampling of the TTAC acquired by simulation. Then, these values reflecting tracer concentration at sampling times were assigned to the corresponding tissues of the segmented VHP image data, so the volume data arranged in time sequence was obtained.

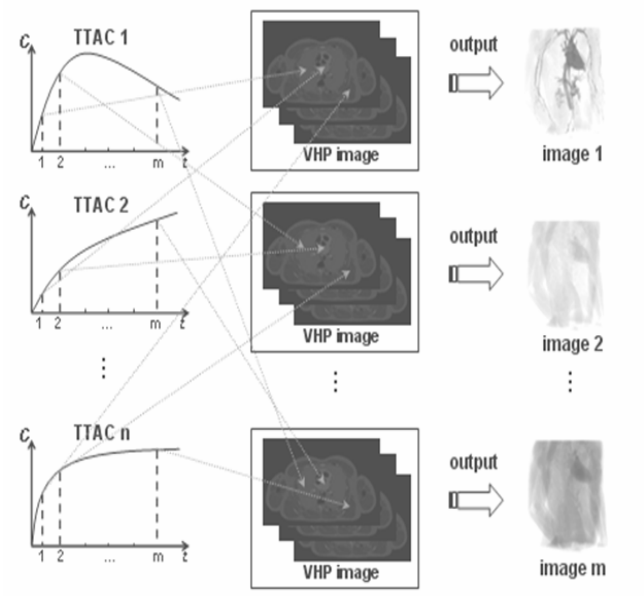

Fig.4. The procedure of visualization. Values sampled from the TACs are assigned to the corresponding tissues of the segmented VHP image data, outputting a number of new image data. “image m” denotes the outputted image data at the *m*th sampling time.

This procedure was equivalent to data mapping from a set of time activity curve (TAC) to the segmented VHP image data, as illustrated in the Fig. 4. Thus a number of new 3D image data which includes the information of the ^{18}F concentration in the tissue was produced at each sampling time. In this mapping, it was assumed that the FDG concentration in one individual tissue was homogeneous under rest condition. Finally, the assigned VHP data were represented in 3D format using volume rendering method (Robb, 1999;

Schroeder, 2001), and some interaction functions were provided in order to observe more conveniently the whole transformation process of the tracer distribution in human body.

The visualization can be performed not only in 2-D format, but also in 3-D format (Fig. 5). The figure shown here used gray colormap, and other colormap can also be used. Certainly, this dynamic process can also be visualized by a sequence of images, or showed as a movie.

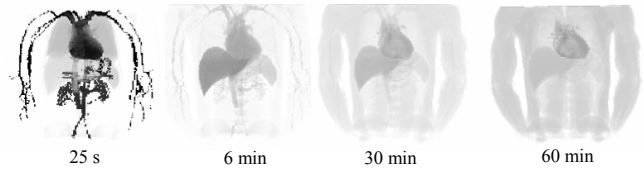

Fig. 5. The 3D visualization result of FDG distribution at the sampling time of 25 s, 6 min, 30min and 60 min, respectively.

3. CONCLUSION

In this study, the FDG distribution kinetics in the tissues of myocardium, lung, liver, stomach, spleen, pancreas, marrow, and kidney, were investigated using dynamic FDG-PET, and the kinetic parameters were estimated. Particular models were established for liver and kidney. For liver, dual-input model was adopted, which accorded with the hepatic physiology and gave a better fitting than the arterial-input model. For kidney, a piecewise model was established to describe the distribution process of FDG. Each individual FDG metabolism model was connected by circulatory system to form a whole body model, which can be used to simulate the FDG metabolic process. The method of simulation and visualization of FDG metabolism based on VHP image provided complete, accurate and direct information of FDG metabolism process in human body. This study was especially for the metabolism of FDG. However, the modelling and visualization methods were for all tracers. The results of this study will be a useful tool for education and research on nuclear imaging. For example, the clinical PET images can be simulated to investigate PET sampling protocol. The results of this study may provide a novel technical platform for the study of pharmacokinetics.

4. ACKNOWLEDGMENT

We are grateful for the people who volunteered for this study. This work was partially supported by the National Nature Science Foundation of China, the Tsinghua-Yue-Yuen Medical Science Foundation, the National Basic Research Program of China, and the Special Research Fund for the Doctoral Program of Higher Education of China, and International Science Linkages established under the Australian Government's innovation statement (CH050131).

REFERENCES

Bertoldo, A., P. Vicini, G. Sambuceti, et al. (1998). Evaluation of compartmental and spectral analysis models of [^{18}F]FDG kinetics for heart and brain studies with PET. *IEEE Transactions on Biomedical Engineering*, **45**, 1429-1448.

Chen, S. and D. Feng (2004). Noninvasive quantification of the differential portal and arterial contribution to the liver blood supply from PET measurements using the ^{11}C-acetate kinetic model. *IEEE Transactions on Biomedical Engineering*, **51**, 1579-1585.

Cui, Y. F., J. Bai (2005). Method of simulation and visualization of FDG metabolism based on VHP image. *Medical Imaging 2005 - Visualization, Image-Guided Procedures, and Display - Proceedings of SPIE. Bellingham: International Society for Optical Engineering*, **5744**, 547-554.

Cui, Y. F., J. Bai, Y. M. Chen and J. H. Tian (2006). Parameter estimation for whole-body kinetic model of FDG metabolism. *Progress in Natural Science*, **16**, 1164-1170.

Cui, Y. F., J. Bai, Y. M. Chen and J. H. Tian (2007a). Kinetic model parameter estimates of liver FDG metabolism. *J Tsinghua Univ (Sci & Tech)*, **47**, 420-423.

Cui, Y. F., J. Bai, Y. M. Chen, J. H. Tian (2007b). A digital model framework of metabolic system based on visible human data set. *International Journal of Image and graphics*, **7**, 143-157.

Gallagher, B.M., A. Ansari, H. Atkins, et al.(1977). Radiopharmaceuticals XXVII. 18F-labeled 2-deoxy-2-fluoro-D-glucose as a radiopharmaceu- tical for measuring regional myocardial glucose metabolism in vivo: tissue distribution and imaging in animals. *J Nucl Med.*, **18**, 990–996.

Hays, M. T. and G. M. Segall (1999). A mathematical model for the distribution of fluorodeoxyglucose in humans. *J Nucl Med.*, **40**, 1358-1366.

Hohne, K. H., B. Pflesser, A. Pommert, M. Riemer, et al. (2001). A realistic model of human structure from the visible human data. *Methods of Information in Medicine*, **40**, 83-89.

Huang, S. C., M. E. Phelps, E. J. Hoffman, K. Sideris, C. J. Selin and D. E. Kuhl (1980). Noninvasive determination of local cerebral metabolic rate of glucose in man. *Am J Physiol Endocrinol Metab*, **238**, E69-82.

Jastrow, H. and L. Vollrath (2003). Teaching and learning gross anatomy using modern electronic media based on the visible human project. *Clinical Anatomy*, **16**, 44-54.

Kostakoglu, L., H. Agress and S. J. Goldsmith (2003). Clinical role of FDG PET in evaluation of cancer patient. *Radiographics*, **23**, 315-340.

Munk, O. L., L. Bass, K. Roelsgaard, et al. (2001). Liver kinetics of glucose analogs measured in pigs by PET: Importance of dual-input blood sampling. *J Nucl Med.*, **42**, 795-801.

Pommert, A., K. H. Hohne, B. Pflesser, E. Richter, et al. (2001). Creating a high-resolution spatial/symbolic model of the inner organs based on the Visible Human. *Medical Image Analysis*, **5**, 221-228.

Reinhardt, M., M. Beu, H. Vosberg, et al. (1999). Quantification of glucose transport and phosphorylation

in human skeletal muscle using FDG PET. *J Nucl Med.*, **40**, 977-985.

Robb, R. A. (1999). 3-D visualization in biomedical applications. *Annual Review of Biomedical Engineering*, **1**, 377-399.

Schroeder, W. J. (2001). *The Visualization Toolkit User's Guide*, Kitware Inc..

Szabo, Z., J. S. Xia, W. B. Mathews, and P. R. Brown (2006). Future direction of renal positron emission tomography. *Seminars in Nuclear Medicine*, **36**, 36-50.